Optics & Laser Technology 163 (2023) 109308

Contents lists available at ScienceDirect

Optics and Laser Technology

journal homepage: www.elsevier.com/locate/optlastec

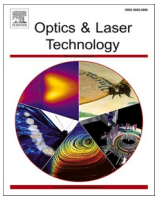

Full length article

How to control the uniform micro bubbles generation on underwater superaerophobic surface?

Xiaodan Gou [a,1], Jinglan Huo [a,1], Qing Yang [b], Yang Cheng [b], Xun Hou [a], Feng Chen [a,*]

[a] State Key Laboratory for Manufacturing System Engineering and Shaanxi Key Laboratory of Photonics Technology for Information, School of Electronic Science and Engineering, Xi'an Jiaotong University, Xi'an 710049, PR China
[b] School of Mechanical Engineering, Xi'an Jiaotong University, Xi'an 710049, PR China

ARTICLE INFO

Keywords:
Femtosecond laser fabrication
Underwater superaerophobic
Micro bubbles
Micro-volcano array

ABSTRACT

Bubbles are an important medium to increase the efficiency of gas/liquid mass transfer. Smaller and more homogeneous bubbles can improve environmental treatment efficiency, microfluidic stability, and medical imaging capabilities. At present, it is still difficult to produce uniform micro bubbles and stably apply them into complex environment. Herein, a strategy of aerating micro bubbles by designing four different structures via laser ablation is proposed. The underwater superaerophobic polyimide (SPI) with micro volcano-like channels has been verified to produce bubbles with a volume of nanoliter. It is attributed to the combination of the micro-nano rough structures covering the surface and the micro-volcanic structure limiting the expansion of bubbles. The SPI with micro volcano-like structure, as a porous aeration film, can make various gases pass, which can be applied to water purification and gas detection. It is also found that the designed SPI with micro volcano-like structure can resist the damage of complex application environments, such as extreme water environments and ultraviolet radiation. As indicated in all the results, the SPI is applicable and flexible. The femtosecond laser can realize high precision and good controllability of the superaerophobic surface, which is difficult for other traditional methods to fabricate micropores. This distinctive membrane provides a new inspiration to design advanced materials for applications in gas transport and collection, wastewater treatment, and chemical reactions. It is also helpful to promote the basic research and applications of micro and nano bubbles generation.

1. Introduction

Bubbles have attractive prospects in water environment remediation [1,2], biomedicine [3–5], and catalysis [6,7]. Besides, bubbles also play a crucial role in micro/nanofabrication [8,9], nanostructuring [10] and nanopatterning [11]. The reduction in bubble size is conducive to increasing the gas/liquid contact area, and thus promoting the reaction efficiency of gas/liquid [12,13]. Many scientists have paid attention to adjust the size of the bubbles for aeration using membranes with uncontrollable porous structure [14–16]. As a result, the sizes of bubbles are irregular. Thus, it is of great significance to prepare a material that could produce bubbles with uniform size and have stable performance in complex environments. Apart from that, a new strategy should be invented to control the size of micro bubbles from the microscopic and theoretical perspective.

Abundant surfaces in nature, such as fish scales and lower surfaces of lotus with micro/nanoscale hierarchical structure, perfectly manifest the repellency of air bubbles [17–19]. Dorrer introduced the concept of "superaerophobicity" for the first time and defined it as the surface on which bubbles formed a large gas contact angle and could move freely [20]. Owing to the excellent property of gas-repelling, underwater superaerophobic surfaces were also successfully prepared for bubble capture and manipulation [21–23], selective passage of bubbles [24–26], and gas/water separation [27,28]. By controlling the existence of the trapped air layer, Huo et al. designed a reversible switching underwater superaerophilic and superaerophobic PTFE surface [29]. Furthermore, Yang et al. fabricated a superaerophobic copper surface with micro/nano structures, on which the bubble could slide freely [30]. In addition, this property can also prevent bubbles from adhering to the surface and reduce the volume of the bubble [30–32]. Yang et al. reported a superaerophobic-hydrophobic membrane modified by polydopamine/polyethyleneimine to decrease the bubble size (0.5 mm) and

* Corresponding author.
E-mail address: chenfeng@mail.xjtu.edu.cn (F. Chen).
[1] Xiaodan Gou and Jinglan Huo contributed equally to this work.

https://doi.org/10.1016/j.optlastec.2023.109308
Received 29 December 2022; Received in revised form 12 February 2023; Accepted 21 February 2023
Available online 9 March 2023
0030-3992/© 2023 Elsevier Ltd. All rights reserved.

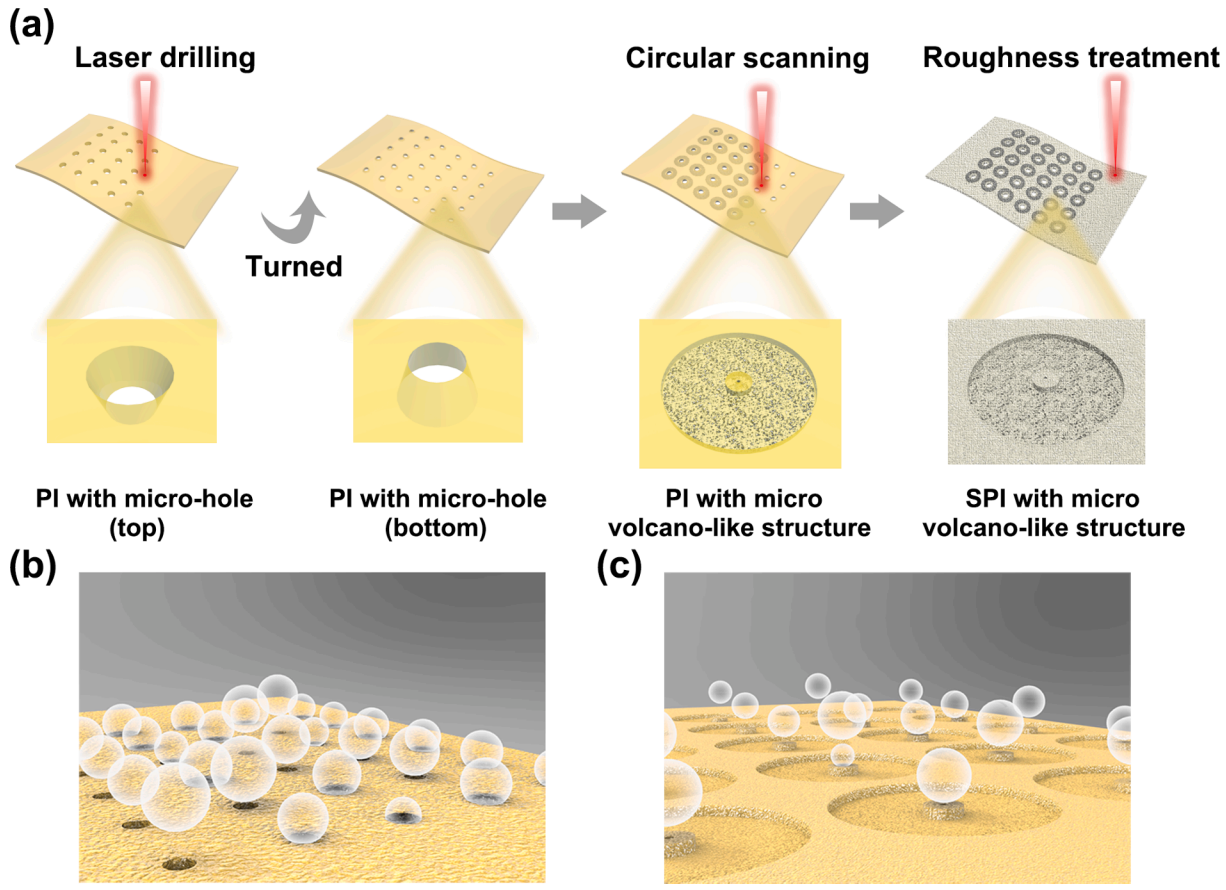

Fig. 1. Preparation process and the principle of different polyimides (PI). (a) Schematic of SPI with micro volcano-like structure. (b) Aeration process using PI with micro-hole structure. (c) Aeration process using SPI with micro volcano-like structure.

enhance the rate of gas/liquid mass transfer [14]. However, the pores of the materials used are randomly distributed. In addition, the location and size of the bubbles cannot be effectively controlled. The femtosecond laser possesses some advantages of ultra-short pulse width and high peak intensity, inducing a minimal heat-affected zone formation [31,33]. Besides, the femtosecond laser is able to process versatile materials [34–36]. Thus, the femtosecond laser is often used to change the surface structure and wettability of the material [25,37–43].

Herein, the femtosecond laser fabrication technique was used to propose a superaerophobic surface that could produce uniform micro bubbles. The micro-holes were firstly formed on the polyimide (PI) surface by laser drilling. Inspired by the structure of volcanos, the micro volcano-like structure was fabricated by taking the micro-hole as the center. Then, based on laser scanning, the underwater superaerophobic PI (SPI) was formed by treating only one side. By comparing four different structures, including smooth hole, rough hole, smooth volcano-like structure and rough volcano-like structure, it was found that the surface with rough volcano-like structure can produce the smallest bubbles due to the underwater superaerophobic characteristic and protuberant micro volcano structure. Beyond that, the resultant SPI with micro volcano-like structure showed low adhesion to bubbles, which eventually formed nanoliter bubbles. With the continuous injection of gas, the formed bubbles can break away from the surface in time and avoid sticking and expanding. Additionally, the SPI can allow various kinds of gases to pass through even oxidizing gases. At the same time, the potential applications in water purification and gas detection were demonstrated. Moreover, the SPI with micro volcano-like structure presented good stability after immersing in acidic/alkaline or salt solutions, UV irradiation, slurry impact, and hydraulic pressure test, which demonstrates its great capability in the gas passage and water treatment fields.

2. Experimental

2.1. Materials

The PI used in our experiment has a thickness of 100 μm (Zhongshan Chenxi Technology Co., Ltd). The methyl orange (MO, Damao Chemical Reagent Factory) was used as a characteristic reagent in the ozone oxidation test. The litmus (Aladdin Co., Ltd) and the bromothymol blue (BTB, 500 mg/L, Aladdin Co., Ltd) were used in carbon dioxide aeration experiments.

2.2. Fabrication of PI with different structures

2.2.1. Fabrication of micro-holes

A femtosecond laser beam (FemtoYSL-20, YSL-photonics, with a pulse duration of 270 fs, central wavelength of 1030 nm) was used. The output femtosecond pulses were 1 kHz. To form the through-micro-holes array, the single-point drilling process was performed to ablate the PI film with the laser power at 26 mW. When the hole was completed, the translation platform moved with a certain distance to the next position to continue drilling.

2.2.2. Fabrication of micro volcano-like structure

Due to the characteristic of the Gaussian beam and the advantages of femtosecond laser ablation [44], the cone-shaped hole will be formed on the PI surface. And the back surface far from the objective lens has a small diameter. Thus, the PI film with micro-hole array was turned. Then with the hole as the center, the volcano-like structure was

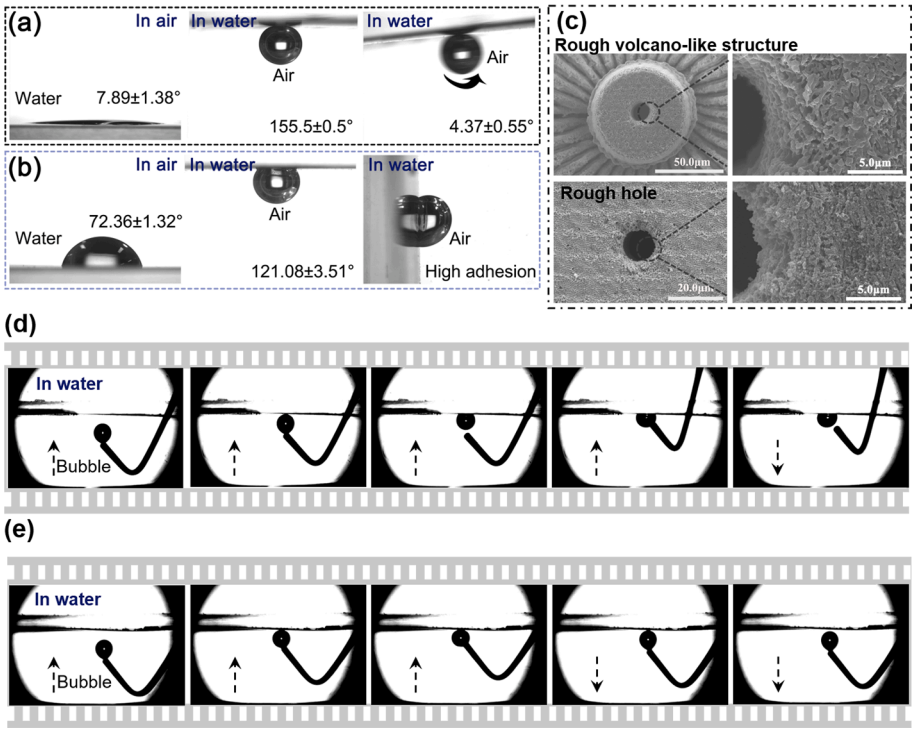

Fig. 2. Wettability and surface morphology of SPI and pristine PI. (a, b) The contact angle of SPI and pristine PI surface, respectively. (c) SEM of rough micro volcano-like structure and rough hole. (d, e) Dynamic adhesion behavior of bubbles on pristine PI and SPI, respectively.

constructed by laser ablation with preprogrammed circular route at the laser power of 8 mW, the scanning speed of 4 mm s^{-1}, and scanning lines interval of 4 μm.

2.2.3. Fabrication of rough surfaces

Finally, the power of the beam was reset to 20 mW. The line-by-line scanning pattern was applied on the surface at a speed of 8 mm s^{-1} and the scanning spacing was 8 μm. The laser pulses used in 2.2.2 and 2.2.3 is from a Ti: sapphire laser system (pulse duration = 50 fs, center wavelength = 800 nm, repetition rate = 1 kHz). The laser beam was focused on the PI film by the objective lens (10X, NA = 0.3, Nikon).

2.3. Characterization

The water contact angle (WCA, ~7 μL), the underwater bubble contact angle (BCA, ~3 μL), and the bubble sliding angle (BSA, ~3 μL) were measured by contact angles measuring system (JC2000D, Powereach, China). Some ultrafast dynamic processes such as bubbling are captured by a high-speed camera (CAMMC1362, Mikrotron, Germany). The microstructures were observed using a scanning electron microscope (FlexSEM1000, Hitachi, Japan). And the three-dimensional (3D) morphology of the micro volcano-like structure was characterized through a laser confocal microscope (LEXT-OLS4000, Olympus, Japan).

3. Results and discussion

3.1. Surface wettability and adhesion

The fabrication process of SPI with micro-volcano array is shown in Fig. 1a. First, the flat and smooth PI film is ablated by the femtosecond laser to produce micro-holes. Since the diameter of the micro-holes formed on the back side of PI is smaller, the PI film is turned for the following processing. Sequentially, the volcano-like structure is formed by ablating the surrounding area with the micro-hole as the center. Finally, the surface is ablated by "line-by-line" scanning, finishing the superaerophobic PI (SPI). During aeration, the SPI with micro volcano-like structures and rough surfaces are more conducive to the formation of small bubbles than hole structures (Fig. 1b and 1c).

The contact pattern between bubbles and the membranes is affected by the wettability of the membranes [45,46]. After laser ablation, the treated PI shows superaerophobicity with WCA of 7.89 ± 1.38° and BCA of 155.5 ± 0.5° (Fig. 2a). The air bubble has low adhesion on the surface and can roll away easily (BSA = 4.37 ± 0.55°). Different from the superaerophobic surface, the untreated PI maintains high bubble adhesion even vertically placed. And the WCA and BCA are measured to be 72.36 ± 1.32° and 121.08 ± 3.51°, respectively (Fig. 2b). The surface of the untreated PI is very smooth without any rough structure (Fig. S1a and b). And the contact area between gas and surface is large (Fig. S2a). While, the rough micro volcano-like structure and the rough hole have a large number of micro and nano rough structures after ablation by laser processing (Fig. 2c, S1c and S1d). And both the rough micro volcano-like structure and the rough hole show superaerophobicity and good bubble rolling properties. Besides, the diameter of the hole formed by the laser ablation is about 15–18 μm, which is the channel for the small bubbles. Due to the action of capillary force, water molecules will enter the micro-nano structure on the surface and form a water film layer when the laser-ablated PI is immersed in water [20,47]. As a result, the laser-ablated PI surface possesses an underwater gas-repellent property, as shown in Fig. S2b. When the original or treated surface is placed at an angle (Fig. S2c), the lateral adhesion force (F_a) can be expressed as follows [48]:

$$F_a = k\omega\gamma_{LV}(\cos\theta_{min} - \cos\theta_{max}) \quad (1)$$

where θ_{min} is the contact angle on the downhill sides, θ_{max} is the contact angle on the uphill sides, k is the retentive force factor, and γ_{LV} is the surface tension of the liquid, and ω is the contact width. From Equation (1), we obtain the speculation that reducing the wettability of the surface would result in diminished contact width and retentive force factor, which finally reduces the adhesive force [49–51]. Thus, bubbles in the rough SPI are more likely to break away from the surface. Under dynamic conditions, the bubble is easily adhered to the membrane surface

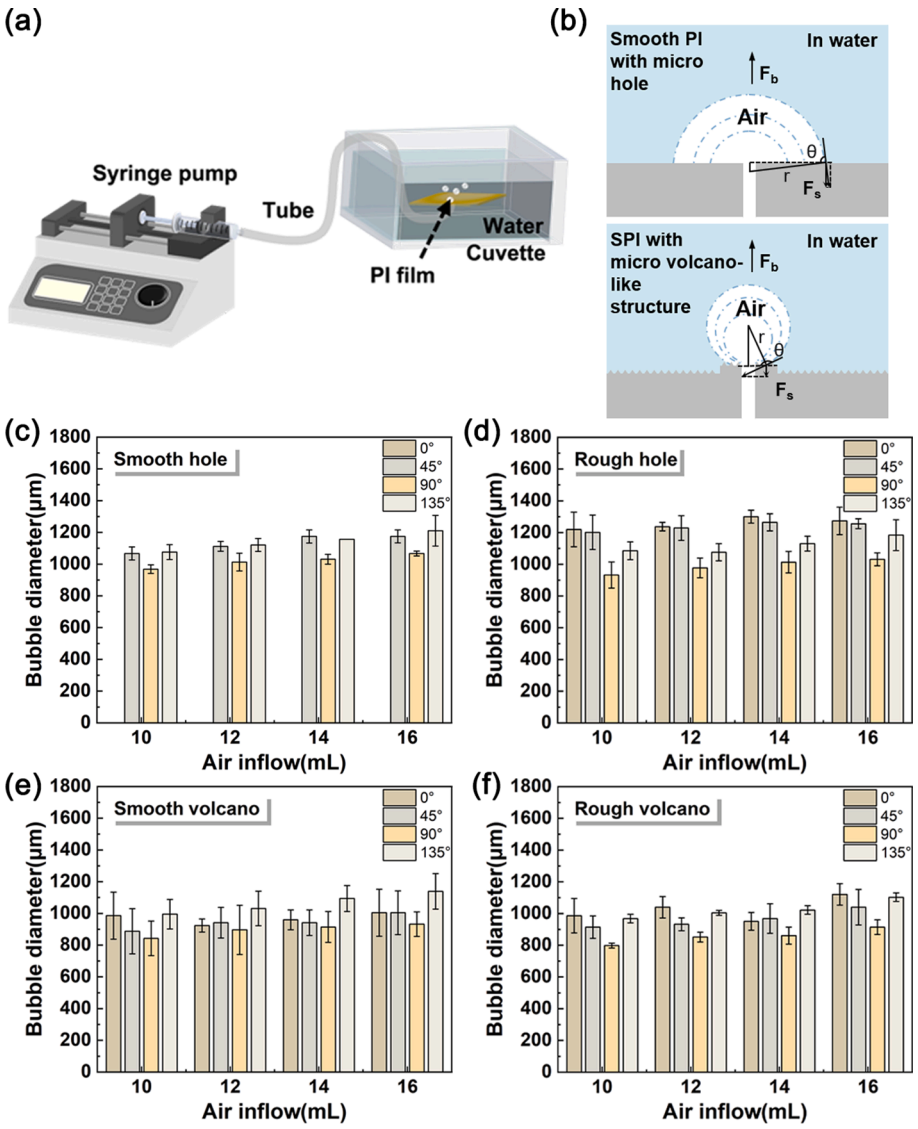

Fig. 3. Schematic diagram of the bubbling process and the size of bubbles produced at different angles on different surfaces. (a) Schematic diagram of the aeration device. (b) Schematic diagram of bubbling process for different surfaces. (c-f) The sizes of bubbles produced on the smooth hole (c), rough hole (d), smooth micro volcano-like structure (e), and rough micro volcano-like structure (f) surfaces under different angles.

when a 3 μL bubble slowly approaches the untreated PI membrane (Fig. 2d and Video S1). Furthermore, the bubble cannot be dragged down even with the assistance of microsyringe, indicating that the adhesion between the bubble and the untreated PI was large (Video S2). On the contrary, the bubbles can move freely as the microsyringe moves up and down and would not cling to the rough PI surface (Fig. 2e and Video S3). This low adhesion avoids the bubbles to adhere to the surface for a long time, which is conducive to the formation of micro bubbles.

3.2. Bubbling and applications in aeration

From the above discussion, it can be seen that the rough surface is beneficial to reduce the adhesion of bubbles, which makes the bubbles detach more quickly. While, the bubbles may expand on the surface with microporous structure during aeration [52]. How to further reduce the adhesion of bubbles to the surface? To solve this problem, we design a micro volcano-like structure based on micro holes. The protruding micro volcano-like structure can limit the range of bubble expansion. In addition, it is beneficial to close the liquid ring near the nozzle in time [53].

As shown in Fig. 3a, the prepared samples were fixed at the end of the bendable tube and placed 0.5–1 cm from the water surface. The bendability of the tube can facilitate the subsequent measurement at different placement angles. The other end of the tube was connected to the syringe (20 mL) and sealed with glue. The syringe was placed on the microinjector pump and the aeration process was controlled by the pump. The bubble sizes were collected and analyzed at a gas injection rate of 1 mL min^{-1} to reduce the influence of velocity of airflow (Fig. S3). The aeration process was captured and recorded by a camera connected to a computer. The sizes of the bubbles produced by four structures, smooth micro hole, rough micro hole, smooth micro volcano-like structure, and rough micro volcano-like structure, are compared. As shown in the Fig. S4, the bubble keeps growing in the process of aeration and adheres to the smooth holes surface for a long time, when it is placed horizontally (0°). And the detached bubbles are irregularly round. Thus, the diameter of it is not counted. By measuring the diameter of the released regular bubbles, it can be seen that under the same experimental conditions, the bubbles generated by the rough hole (Fig. 3d) are smaller than the smooth hole (Fig. 3c), which also verifies that the rough surface is conducive to the generation of micro bubbles. In terms of the structure, the overall diameter of the bubbles produced by the micro volcano-like structures (Fig. 3e and 3f) is smaller and more uniform than

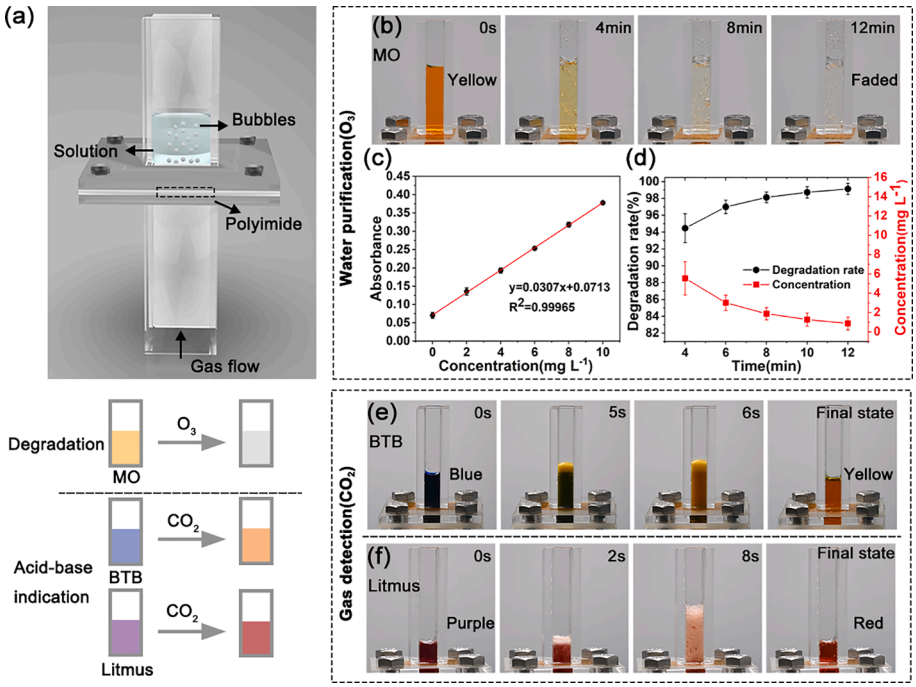

Fig. 4. Aeration experiment for water purification and gas detection. (a) Diagram of aeration device and process. (b) Ozone degradation experiment of MO. (c) Standard curve of MO used in the experiment. (d) Decolorization and degradation rate of MO. (e) Discoloration experiment of BTB. (f) Discoloration experiment of litmus.

that of holes. Furthermore, the bubbles produced by the rough micro volcano-like structure are the smallest. To understand the force between the bubbles and the surface, the state is assumed to be a quasi-static manner [14]. The behavior of bubble mainly depends on surface adhesion force F_s (an axial component of surface tension) and buoyancy force F_b(Fig. 3b). The radial component of surface tension and bubble gravity can be ignored. With the injection of gas, the radius r of the bubble continues to become larger. Assuming that the bubble is spherical, the buoyancy force F_b obeys the positive correlation to ther^3. Besides, the F_s is also related with growth of the bubbles, which can be described by the following Equation [54]:

$$F_s = 2\pi\gamma_{LV} r_c \sin\theta \tag{2}$$

where θ is the bubble contact angle, r_c is the equal to $r\sin\theta$ and stands for the contact radius of the bubble with the surface and γ_{LV} is the surface tension of the liquid. Generally, the contact radius in aerophilic surface tends to expand. Thus, both F_b and F_s increase with an increasing of the bubble size. According to the above discussion, F_b increases faster thanF_s. The bubbles can break away from the surface when F_b is greater than F_s [14]. This is more likely to result in a larger volume of bubbles. While, in the SPI surface, its contact radius is shorter than that on the smooth surface. Besides, with the increase of bubble contact angle, the contact radius changes little and the F_s becomes smaller. At the same time, the F_b increases with bubble size. Thus, bubbles can leave the surface as soon as possible with small size.

The sample is subjected to different forces at different tilt angles, which affects the size of the generated bubbles. Four types of PI films are also placed at different angles (45°, 90°, 135°) for aeration. As illustrated in Fig. 3c-3f, the bubble size is the smallest when PI is placed vertically (90°). The diameter of bubbles is approximately 797.9 ± 15.5 μm and the volume is 264.1 nL, as for the surface with rough micro volcano-like structure (Fig. 3f and Fig. S5). And the volume of bubbles is relatively uniform. From the 3D morphology, the volcano structure is higher than the surrounding surface, which reduces the contact area of bubbles and prevents the expansion of bubbles (Fig. S6). It can be seen that both surface wettability and aeration structure have an effect on the size of the bubbles.

To characterize the aeration process vividly, O_3 or CO_2 gas is injected to pass through an aeration device equipped with PI with an array of volcano-like structures into different solutions (MO, BTB, and litmus) for degradation and acid-base indication, as shown in Fig. 4a. The interval between two volcano-like structure is 1200 μm. Since ozone is often used in wastewater treatment [55–57], we tested the aeration process of ozone gas (Fig. 4b and Video S4). Firstly, 100 mg/L MO solution is prepared. Then, the solutions with an equal gradient concentration (2 mg/L) are prepared. The maximum absorption wavelength is determined to be 462 nm by scanning test using a microplate reader and the standard working curve is plotted. The correlation coefficient R^2 is 0.99965, which means that the curve fits well (Fig. 4c). The absorbance of the solution under different aeration times is measured, and the concentration is calculated according to the standard curve. And then the decolorization rate and removal rate are calculated according to Equation (3) and (4).

$$\text{Decolorization rate} = \frac{A_0 - A_t}{A_0} * 100\% \tag{3}$$

$$\text{Removal rate} = \frac{C_0 - C_t}{C_0} * 100\% \tag{4}$$

where A_0 and C_0 in the Equations are the absorbance and concentration of MO before treatment, and A_t and C_t are the absorbance and concentration of MO after aeration. From Fig. 4d, the concentration of MO is reduced from 100 mg/L to 0.8 mg/L after 12 min of aeration. It shows that the SPI has good permeability to oxidizing gas. The results of this experiment show that the SPI has a promising application in wastewater purification. Besides, this material can achieve the detection and identification of specific gases by color change experiments. With the continuous supply of CO_2, a large number of fine bubbles emerge, generating the carbonic acid and reducing the pH of the solution. The color of the BTB solution changes from blue to yellow in 6 s (Fig. 4e and Video S5). For the litmus solvent, the solution changes from purple to red quickly after the supply of CO_2 (Fig. 4f and Video S6). The above

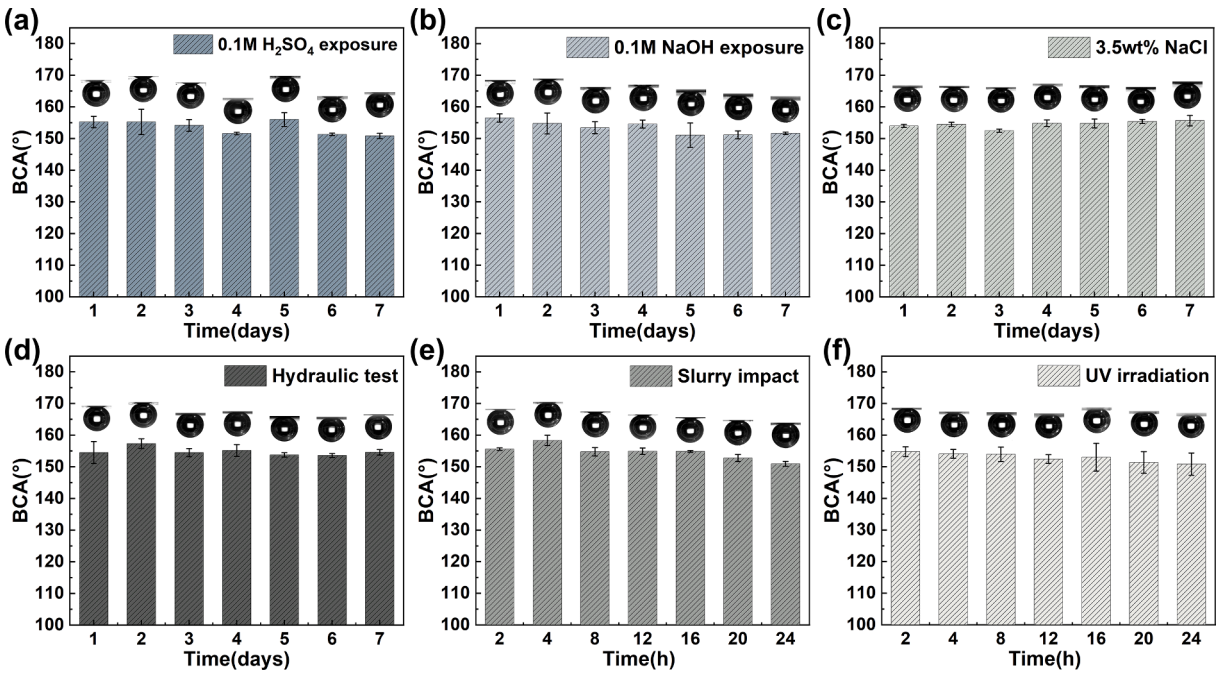

Fig. 5. The stability of SPI in different environments. (a) In 0.1 M H_2SO_4 solution. (b) In 0.1 M NaOH solution. (c) In 3.5 wt% NaCl solution. (d) Immersed under 30 m water pressure. (e) Slurry impact. (f) UV irradiation.

results show that this membrane is suitable for a wide range of gases for water purification and gas detection field.

3.3. Stability of SPI in potential application environments

In real-world applications, aeration may occur in various water environments as well as atmospheric environments. Herein, different environments are simulated to evaluate the stability of the prepared materials. As depicted in Fig. 5a and 5b, the SPI retains good superaerophobicity after being immersed in acidic/alkaline solutions (0.1 M H_2SO_4 or 0.1 M NaOH) solutions for 7 days, demonstrating its good long-term stability. In addition, the BCA can maintain above 150° even after 7 days of immersion in 3.5 wt% salt solution, or under 30 m water pressure environment (Fig. 5c and 5d). In addition, the sand smaller than 40 mesh is sifted out by a metal mesh and configured into 2 % mixture of sand and water. The mixture is stirred at 500 rpm. The SPI is suspended in the center of the water stream and is continuously impacted. From the result, the SPI could still exhibit excellent air repellency after being scoured for 24 h (Fig. 5e). Besides, the UV irradiation experiment is performed by putting the SPI at a distance of 10 cm under the UV lamp (360–365 nm) at a power of 60 W for irradiation. The SPI is exposed for 24 h and can still keep its superaerophobicity (Fig. 5f). These tests in extreme conditions demonstrate the suitability and flexibility of SPI surfaces for practical applications.

4. Conclusions

In summary, a strategy to design the superaerophobic surface was developed based on the femtosecond laser treatment. Four materials with different surface structures were tested. The SPI with micro volcano-like structure has a WCA of 7.89 ± 1.38°, BCA of 155.5 ± 0.5°, and BSA of 4.37 ± 0.55°. Under certain pressure, bubbles will not stick to the surface and are prone to roll easily, showing excellent low-adhesive superaerophobicity. The designed surface can be used as a microporous membrane for aeration, which can lead to uniform micro bubbles. Such a membrane material can also allow the passage of various gases, even those with strong oxidizing properties, which can be used in water treatment and the gas inspection. The SPI shows excellent resistance to complex application conditions, including UV irradiation, slurry impact, hydraulic test, and corrosive solutions. This designed surface is expected to have great significance for various applications in gas transport and collection, wastewater treatment, and chemical reactions.

CRediT authorship contribution statement

Xiaodan Gou: Conceptualization, Methodology, Investigation, Validation, Data curation, Writing – original draft. **Jinglan Huo:** Methodology, Investigation, Writing – review & editing. **Qing Yang:** Resources, Supervision, Project administration, Writing – review & editing. **Yang Cheng:** Methodology, Data curation, Writing – review & editing. **Xun Hou:** Supervision. **Feng Chen:** Resources, Supervision, Conceptualization, Writing – review & editing, Project administration, Funding acquisition.

Declaration of Competing Interest

The authors declare that they have no known competing financial interests or personal relationships that could have appeared to influence the work reported in this paper.

Data availability

Data will be made available on request.

Acknowledgements

This work is supported by the National Science Foundation of China under the Grant nos. 12127806, 61875158, 62175195, the International Joint Research Laboratory for Micro/Nano Manufacturing and Measurement Technologies, the Fundamental Research Funds for the Central Universities.

Appendix A. Supplementary material

Supplementary data to this article can be found online at https://doi.

org/10.1016/j.optlastec.2023.109308.

References

[1] W. Fan, J. Cui, Q. Li, Y. Huo, D. Xiao, X. Yang, H. Yu, C. Wang, P. Jarvis, T. Lyu, M. Huo, Bactericidal efficiency and photochemical mechanisms of micro/nano bubble-enhanced visible light photocatalytic water disinfection, Water Res. 203 (2021), 117531.

[2] B. Chen, S. Zhou, N. Zhang, H. Liang, L. Sun, X. Zhao, J. Guo, H. Lu, Micro and nano bubbles promoted biofilm formation with strengthen of cod and tn removal synchronously in a blackened and odorous water, Sci. Total Environ. 837 (2022), 155578.

[3] A. Shakeri-Zadeh, H. Zareyi, R. Sheervalilou, S. Laurent, H. Ghaznavi, H. Samadian, Gold nanoparticle-mediated bubbles in cancer nanotechnology, J Control Release 330 (2021) 49–60.

[4] R. Xiong, R.X. Xu, C. Huang, S. De Smedt, K. Braeckmans, Stimuli-responsive nanobubbles for biomedical applications, Chem. Soc. Rev. 50 (2021) 5746–5776.

[5] A.M. Rather, Y. Xu, Y. Chang, R.L. Dupont, A. Borbora, U.I. Kara, J.C. Fang, R. Mamtani, M. Zhang, Y. Yao, S. Adera, X. Bao, U. Manna, X. Wang, Stimuli-responsive liquid-crystal-infused porous surfaces for manipulation of underwater gas bubble transport and adhesion, Adv. Mater. 34 (2022) 2110085.

[6] J. Hou, C. Ji, G. Dong, B. Xiao, Y. Ye, V. Chen, Biocatalytic janus membranes for CO_2 removal utilizing carbonic anhydrase, J. Mater. Chem. A 3 (2015) 17032–17041.

[7] M. Li, J. Wei, L. Ren, Y. Zhao, Z. Shang, D. Zhou, W. Liu, L. Luo, X. Sun, Superwetting behaviors at the interface between electrode and electrolyte, Cell Reports Physical Science 2 (2021), 100374.

[8] G. Li, S. Jia, H. Yang, J. Chen, Direction-controllable plasmonic color scanning by using laser-induced bubbles, Adv. Funct. Mater. 31 (2021) 2008579.

[9] D. Zhang, B. Ranjan, T. Tanaka, K. Sugioka, Underwater persistent bubble-assisted femtosecond laser ablation for hierarchical micro/nanostructuring, Int. J. Extrem. Manuf. 2 (2020), 015001.

[10] M. Senegačnik, P. Gregorčič, Diffraction-driven laser surface nanostructuring: Towards patterning with curved periodic surface structures, Appl. Surf. Sci. 610 (2023) 155486.

[11] S. Fujii, R. Fukano, Y. Hayami, H. Ozawa, E. Muneyuki, N. Kitamura, M.-A. Haga, Simultaneous formation and spatial patterning of ZnO on ITO surfaces by local laser-induced generation of microbubbles in aqueous solutions of $[Zn(NH_3)_4]^{2+}$, ACS Appl. Mater. Interfaces 9 (2017) 8413–8419.

[12] Z. Yang, J. Cheng, R. Lin, J. Zhou, K. Cen, Improving microalgal growth with reduced diameters of aeration bubbles and enhanced mass transfer of solution in an oscillating flow field, Bioresour. Technol. 211 (2016) 429–434.

[13] A. Azevedo, H. Oliveira, J. Rubio, Bulk nanobubbles in the mineral and environmental areas: Updating research and applications, Adv. Colloid Interface Sci. 271 (2019), 101992.

[14] H.C. Yang, J. Hou, L.S. Wan, V. Chen, Z.K. Xu, Janus membranes with asymmetric wettability for fine bubble aeration, Adv. Mater. Interfaces 3 (2016) 1500774.

[15] G.J. Wang, B.H. Wu, Z.K. Xu, L.S. Wan, Janus polymer membranes prepared by single-side polydopamine deposition for dye adsorption and fine bubble aeration, Mater. Chem. Front. 3 (2019) 2102–2109.

[16] B. Wang, X. Xiong, Y. Shui, Z. Huang, K. Tian, A systematic study of enhanced ozone mass transfer for ultrasonic-assisted ptfe hollow fiber membrane aeration process, Chem. Eng. J. 357 (2019) 678–688.

[17] J. Wang, Y. Zheng, F.Q. Nie, J. Zhai, L. Jiang, Air bubble bursting effect of lotus leaf, Langmuir 25 (2009) 14129–14134.

[18] J. Yong, F. Chen, Q. Yang, J. Huo, X. Hou, Superoleophobic surfaces, Chem. Soc. Rev. 46 (2017) 4168–4217.

[19] J. Yong, F. Chen, J. Huo, Y. Fang, Q. Yang, H. Bian, W. Li, Y. Wei, Y. Dai, X. Hou, Green, biodegradable, underwater superoleophobic wood sheet for efficient oil/water separation, ACS Omega 3 (2018) 1395–1402.

[20] C. Dorrer, J. Ruhe, Superaerophobicity: Repellence of air bubbles from submerged, surface-engineered silicon substrates, Langmuir 28 (2012) 14968–14973.

[21] J. Huo, X. Bai, J. Yong, Y. Fang, Q. Yang, X. Hou, F. Chen, How to adjust bubble's adhesion on solid in aqueous media: Femtosecond laser-ablated patterned shape-memory polymer surfaces to achieve bubble multi-manipulation, Chem. Eng. J. 414 (2021), 128694.

[22] J. Yong, Q. Yang, J. Huo, X. Hou, F. Chen, Underwater gas self-transportation along the femtosecond laser-written open superhydrophobic surface microchannels (<100 μm) for bubble/gas manipulation, Int. J. Extrem. Manuf. 4 (2021), 015002.

[23] S. Ben, Y. Ning, Z. Zhao, Q. Li, X. Zhang, L. Jiang, K. Liu, Underwater directional and continuous manipulation of gas bubbles on superaerophobic magnetically responsive microcilia array, Adv. Funct. Mater. 32 (2022) 2113374.

[24] J. Yong, F. Chen, Y. Fang, J. Huo, Q. Yang, J. Zhang, H. Bian, X. Hou, Bioinspired design of underwater superaerophobic and superaerophilic surfaces by femtosecond laser ablation for anti- or capturing bubbles, ACS Appl Mater Interfaces 9 (2017) 39863–39871.

[25] Z. Wu, K. Yin, J. Wu, Z. Zhu, J.A. Duan, J. He, Recent advances in femtosecond laser-structured janus membranes with asymmetric surface wettability, Nanoscale 13 (2021) 2209–2226.

[26] K. Yin, S. Yang, X. Dong, D. Chu, J.A. Duan, J. He, Robust laser-structured asymmetrical ptfe mesh for underwater directional transportation and continuous collection of gas bubbles, Appl. Phys. Lett. 112 (2018), 243701.

[27] J. Yong, Q. Yang, J. Huo, X. Hou, F. Chen, Superwettability-based separation: From oil/water separation to polymer/water separation and bubble/water separation, Nano Select 2 (2021) 1580–1588.

[28] C. Pei, Y. Peng, Y. Zhang, D. Tian, K. Liu, L. Jiang, An integrated janus mesh: Underwater bubble antibuoyancy unidirectional penetration, ACS Nano 12 (2018) 5489–5494.

[29] J. Huo, J. Yong, F. Chen, Q. Yang, Y. Fang, X. Hou, Trapped air-induced reversible transition between underwater superaerophilicity and superaerophobicity on the femtosecond laser-ablated superhydrophobic ptfe surfaces, Adv. Mater. Interfaces 6 (2019) 1900262.

[30] S. Yang, K. Yin, X. Dong, J. He, J.A. Duan, Laser structuring of underwater bubble-repellent surface, J Nanosci Nanotechnol 18 (2018) 8381–8385.

[31] J. Yong, Q. Yang, X. Hou, F. Chen, Nature-inspired superwettability achieved by femtosecond lasers, Ultrafast Science (2022) 1–51.

[32] J. Bernardini, U. Sen, M. Jafari Gukeh, P. Asinari, C.M. Megaridis, Wettability-engineered meshes for gas microvolume precision handling in liquids, ACS Appl Mater Interfaces 12 (2020) 18046–18055.

[33] Z. Lin, M. Hong, Femtosecond laser precision engineering: From micron, submicron, to nanoscale, Ultrafast Science 2021 (2021) 9783514.

[34] K. Yin, Z. Wu, J. Wu, Z. Zhu, F. Zhang, J.A. Duan, Solar-driven thermal-wind synergistic effect on laser-textured superhydrophilic copper foam architectures for ultrahigh efficient vapor generation, Appl. Phys. Lett. 118 (2021), 211905.

[35] K. Yin, D. Chu, X. Dong, C. Wang, J.A. Duan, J. He, Femtosecond laser induced robust periodic nanoripple structured mesh for highly efficient oil-water separation, Nanoscale 9 (2017) 14229–14235.

[36] Y. He, L. Wang, T. Wu, Z. Wu, Y. Chen, K. Yin, Facile fabrication of hierarchical textures for substrate-independent and durable superhydrophobic surfaces, Nanoscale 14 (2022) 9392–9400.

[37] S. Zhu, J. Li, S. Cai, Y. Bian, C. Chen, B. Xu, Y. Su, Y. Hu, D. Wu, J. Chu, Unidirectional transport and effective collection of underwater CO_2 bubbles utilizing ultrafast-laser-ablated janus foam, ACS Appl Mater Interfaces 12 (2020) 18110–18115.

[38] J. Huo, Q. Yang, J. Yong, P. Fan, Y.f. Lu, X. Hou, F. Chen, Underwater superaerophobicity/superaerophilicity and unidirectional bubble passage based on the femtosecond laser-structured stainless steel mesh, Adv. Mater. Interfaces 7 (2020) 1902128.

[39] F. Chen, Z. Deng, Q. Yang, H. Bian, G. Du, J. Si, X. Hou, Rapid fabrication of a large-area close-packed quasi-periodic microlens array on BK7 glass, Opt. Lett. 39 (2014) 606–609.

[40] H. Liu, F. Chen, X. Wang, Q. Yang, D. Zhang, J. Si, X. Hou, Photoetching of spherical microlenses on glasses using a femtosecond laser, Opt. Commun. 282 (2009) 4119–4123.

[41] D. Zhang, F. Chen, Q. Yang, J. Si, X. Hou, Mutual wetting transition between isotropic and anisotropic on directional structures fabricated by femotosecond laser, Soft Matter 7 (2011) 8337–8342.

[42] S. He, F. Chen, K. Liu, Q. Yang, H. Liu, B. Hao, X. Meng, S. Chao, J. Si, Y. Zhao, H. Xun, Fabrication of three-dimensional helical microchannels with arbitrary length and uniform diameter inside fused silica, Opt. Lett. 37 (2012) 3825–3827.

[43] L. Wang, K. Yin, Q. Deng, Q. Huang, J. He, J.A. Duan, Wetting ridge-guided directional water self-transport, Adv Sci 9 (2022) 2204891.

[44] C. Chen, L.A. Shi, Z. Huang, Y. Hu, S. Wu, J. Li, D. Wu, J. Chu, Microhole-arrayed pdms with controllable wettability gradient by one-step femtosecond laser drilling for ulltrafast underwater bubble unidirectional self-transport, Adv. Mater. Interfaces 6 (2019) 1900297.

[45] J. Park, J. Ryu, S.J. Lee, Penetration of a bubble through porous membranes with different wettabilities, Soft Matter 15 (2019) 5819–5826.

[46] Y. Xia, X. Gao, R. Li, Influence of surface wettability on bubble formation and motion, Langmuir 37 (2021) 14483–14490.

[47] J. Yong, S.C. Singh, Z. Zhan, F. Chen, C. Guo, How to obtain six different superwettabilities on a same microstructured pattern: Relationship between various superwettabilities in different solid/liquid/gas systems, Langmuir 35 (2019) 921–927.

[48] R. Ozbay, A. Kibar, C.H. Choi, Bubble adhesion to superhydrophilic surfaces, in: Advances in contact angle, wettability and adhesion, 2015.

[49] J.E. George, S. Chidangil, S.D. George, Recent progress in fabricating superaerophobic and superaerophilic surfaces, Adv. Mater. Interfaces 4 (2017) 1601088.

[50] C. Huang, Z. Guo, The wettability of gas bubbles: From macro behavior to nano structures to applications, Nanoscale 10 (2018) 19659–19672.

[51] B. Su, Y. Tian, L. Jiang, Bioinspired interfaces with superwettability: From materials to chemistry, J. Am. Chem. Soc. 138 (2016) 1727–1748.

[52] J. Tang, Y. Zhang, Y. Yao, N. Dai, Z. Ge, D. Wu, High-performance ultrafine bubble aeration on janus aluminum foil prepared by laser microfabrication, Langmuir 37 (2021) 6947–6952.

[53] J. Yong, S.C. Singh, Z. Zhan, J. Huo, F. Chen, C. Guo, Reducing adhesion for dispensing tiny water/oil droplets and gas bubbles by femtosecond laser-treated needle nozzles: Superhydrophobicity, superoleophobicity, and superaerophobicity, ChemNanoMat 5 (2019) 241–249.

[54] Z. Lu, Y. Li, X. Lei, J. Liu, X. Sun, Nanoarray based "superaerophobic" surfaces for gas evolution reaction electrodes, Mater. Horizons 2 (2015) 294–298.

[55] Z. Xia, L. Hu, Treatment of organics contaminated wastewater by ozone micro-nano-bubbles, Water 11 (2019) 55.

[56] C. Zhang, M. Cao, H. Ma, C. Yu, K. Li, C. Yu, L. Jiang, Morphology-control strategy of the superhydrophobic poly(methyl methacrylate) surface for efficient bubble adhesion and wastewater remediation, Adv. Funct. Mater. 27 (2017) 1702020.

[57] L. Wang, S. Song, L. Xu, N.J.D. Graham, W. Yu, Beneficial role of pre- and post-ozonation in a low rate biofiltration-ultrafiltration process treating reclaimed water, Water Res. 226 (2022), 119284.